Probing Intra- versus Interchain Kinetic Preferences of L-Thr Acylation on Dimeric VibF with Mass Spectrometry

Leslie M. Hicks,* Carl J. Balibar,† Christopher T. Walsh,† Neil L. Kelleher,* and Nathan J. Hillson‡
*Department of Chemistry, University of Illinois at Urbana-Champaign, Urbana, Illinois; †Department of Biological Chemistry and Molecular Pharmacology, Harvard Medical School, Boston, Massachusetts; and ‡Department of Developmental Biology, Stanford University School of Medicine, Stanford, California

ABSTRACT We present a method to probe intra- and interchain activities within dimeric nonribosomal peptide synthetases. Utilizing domain inactivation and analytical mass mutants in conjunction with rapid-quench, mass spectrometry, and a probabilistic kinetic model, we have elucidated the pre-steady-state intra- and interchain rates and the corresponding flux of the acylation of L-Thr onto VibF. Although the intra rate is significantly faster than the inter rate, the data are most consistent with an even flux of covalent substrate loading where neither pathway dominates. These pre-steady-state results confirm previous steady-state in vitro mutant complementation studies of VibF. Extension of this methodology to other dimeric nonribosomal peptide synthetases, and to the related fatty acid and polyketide synthases, will further our biophysical understanding of their acyl-intermediate-processing pathways.

INTRODUCTION

Many important natural products are biosynthesized by nonribosomal peptide synthetases (NRPSs), fatty acid synthases (FASs), and polyketide synthases (PKSs), and much effort has been placed on understanding the mechanisms of such functionally complex systems. Despite the diversity of their products, the overall macromolecular structure and organization of these enzymes are very similar. They consist of individual or multiple modules comprised of several domains, each of which is responsible for one or more of the catalytic activities necessary for the incorporation and tailoring of an amino acid (NRPS) or acyl-CoA (PKS/FAS) monomer into the elongating cascade of acyl-*S*-enzyme intermediates (1–4). Although FASs are unimodular and iterative in nature (5), NRPSs and type I PKSs contain multiple modules, usually arranged colinearly, that form an ''assembly line'' to synthesize their final product (6).

Characterization of the quaternary structure of NRPSs, FASs, and PKSs is not only important for understanding how modules and domains interact, but is also of interest because higher-order oligomeric structural arrangements allow for alternate paths of elongation, as the cascade of intermediates can flow in *cis* (intrachain) or *trans* (interchain) along the several active sites of the enzyme. Although solution/crystal structures and homology models have been determined for individual domains (7–14) and the structures of mammalian and fungal FAS have recently been elucidated at ~5 Å resolution (15,16), high-resolution crystal structures have yet to be reported for an entire NRPS, FAS, or PKS module. It has been shown that FAS (17–21) and deoxyerythronolide B synthase PKS subunits (22–24) are obligate homodimers and can operate through both intra- and interchain elongation cycles. Topology has been additionally investigated by an in vitro mutant complementation strategy where catalytically active heterodimers can be formed from two differentially modified inactive homodimers (23–27). Various models have been proposed to describe the organization of the oligomeric state of these megasynthases, including head-to-tail dimers and head-to-head interwound helical dimers (5,22). Smith and co-workers recently reported the engineering of an active animal FAS dimer with only one competent subunit (28). This information, in combination with reexamination of the specificity of cross-linking (14) and recent cryoelectron microscopy analysis (29–32), has resulted in the proposal of a revised head-to-head coiled arrangement for FAS (14,32).

There remains considerable uncertainty over the higher-order structure of NRPSs in general (33,34), but it has been shown that the VibF subunit of vibriobactin synthetase is dimeric (33). Vibriobactin synthetase (Fig. 1) is a four-subunit NRPS system responsible for synthesizing an iron-chelating catechol siderophore that contributes to a system of iron acquisition essential for virulence of *Vibrio cholerae* during vertebrate infection (35). The ordering of domains within VibF (Cy1-Cy2-A-C1-PCP-C2) deviates from the canonical NRPS repeat (C-A-PCP) and contains a condensation domain (C1) in a location that is usually reserved for modifying domains. After biochemical reconstitution of the full assembly line for vibriobactin production allowed for the assignment of function to the six domains of VibF, it was determined that C1 is catalytically inactive (36). Although somewhat common in PKSs (37–39), NRPSs rarely contain catalytically inactive domains (40–42). Deletion of the C1 domain results in the formation of two subfragments (Cy1-Cy2-A and PCP-C2) of VibF, which together can fully

Submitted March 10, 2006, and accepted for publication June 19, 2006.

Leslie M. Hicks and Carl J. Balibar contributed equally to this work.

Address reprint requests to Nathan J. Hillson, Dept. of Developmental Biology, Stanford University School of Medicine, Stanford, CA 94305-5427. E-mail: hillson@gmail.com.

0006-3495/06/10/2609/11 $2.00

doi: 10.1529/biophysj.106.084848

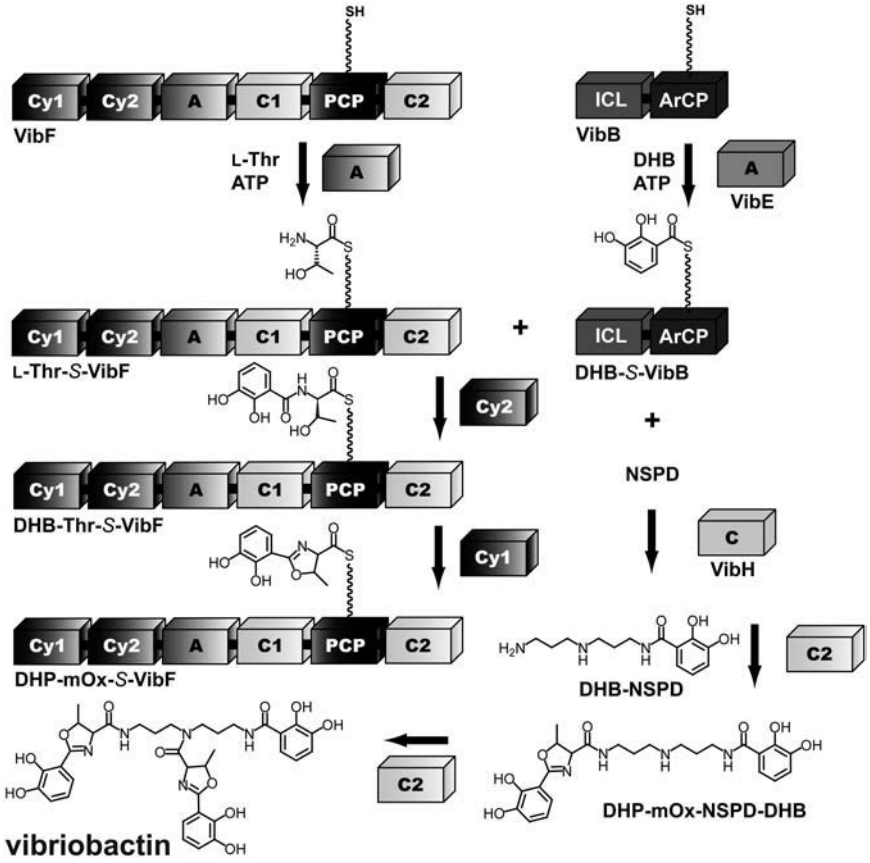

FIGURE 1 Overview of vibriobactin biosynthesis. Vibriobactin is synthesized from two molecules of L-Thr, three molecules of 2,3 dihydroxybenzoate, and one molecule of norspermidine by a four-component NRPS comprising VibB, VibE, VibF, and VibH.

reconstitute vibriobactin production but no longer form a higher-order structure. It was shown that although the C1 domain plays no catalytic role, it is primarily responsible for the dimerization of VibF and may properly position neighboring domains to enhance catalytic activity (42). Previous in vitro mutant complementation studies of VibF revealed that the Cy1, Cy2, A, and C2 domains can perform their activities in both intra- and interchain fashions, and that the Cy1, Cy2, and A domains show no clear preference for intra- or interchain activity when overall vibriobactin production rates are monitored (33). However, the steady-state detection of any such kinetic preferences via in vitro mutant complementation could be suppressed by a subsequent slow step, and the rate-limiting step performed by VibF has not been identified.

Here we introduce a mass spectrometric approach coupled with a probabilistic kinetic model to probe the intra- and interchain rates and corresponding flux within dimeric NRPS, FAS, and PKS enzyme complexes, demonstrating proof of principle through application of this methodology to the dimeric NRPS module VibF. Using high-resolution mass spectrometry (MS), we assayed the acylation of the peptidyl carrier protein (PCP) with L-Thr, catalyzed by the adenylation (A) domain. Distinct enzymatic activities were monitored by mixing two constructs, an analytical mass mutant in the PCP domain (hereafter denoted by PCP_a) and a catalytically inactive A domain mutant (33) (hereafter denoted by A*), to yield homo- and heterodimers of PCP_a and A* (Fig. 2). The analytical mass mutation to the PCP domain was designed to not affect function, at the same time allowing intermediates tethered to a PCP_a domain to be distinguishable by MS from those tethered to a wild-type PCP. Such mixtures of PCP_a and A* interrogated in the pre-steady-state revealed the rates of VibF intra- and interchain acylation and to what extent L-Thr is transferred through each pathway. Features of high-resolution MS, such as high mass accuracy (typically <1 Da) and the ability to obtain semiquantitative regiospecific information, facilitate its use as a largely unbiased measurement tool to unambiguously interrogate the covalent catalysis executed by thiotemplate enzymes in the biosynthesis of many therapeutically interesting natural products.

MATERIALS AND METHODS

Design and purification of VibF mutants

The gene for the analytical PCP_a mutant was constructed via the method of splicing by overlap extension (SOE) (43) using pVibF (35) plasmid as the template. The accession number for the complete VibF sequence is AF287255. In the first round of PCR amplification, the 5′ fragment of the mutant was amplified using the primers 5′-GGTGACTTGGTTAGTGGATCCTCCAGTGCATC-3′ and 5′-CAAGCGACCAATGAC**TGT**CGTTGCGATCAGGG-3′ and the 3′ fragment of the mutant was amplified using the

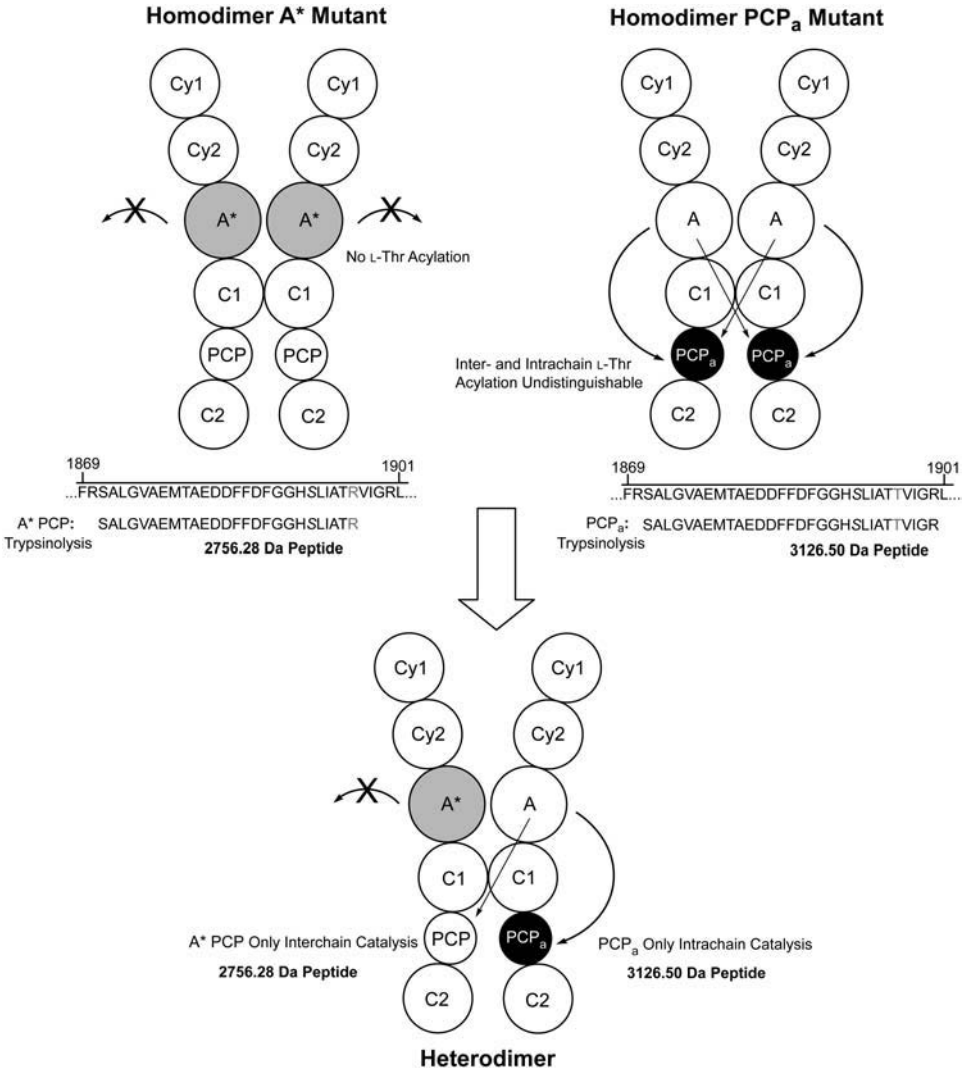

FIGURE 2 Scheme for A*PCP + PCP_a mixing experiment. Homodimers of the A* mutant are unable to undergo catalysis, and A domains from homodimers of the PCP_a mutant perform both intra- and interchain acylation. Mixing of the two species to form heterodimers results in the A*PCP undergoing only interchain acylation and the PCP_a undergoing only intrachain acylation. The two PCP fragments can be resolved by MS after trypsinolysis due to the analytical mass mutation introduced into the PCP_a fragment, which increases its mass by 370.22 Da.

primers 5′-CCCTGATCGCAACG**ACA**GTCATTGGTCGCTTG-3′ and 5′-GTTCATCACGTACGAAATTGAGTC-3′ (bold print indicates mutations). After PCR purification the two fragments were mixed together and further amplified using the forward primer from the 5′ fragment and the reverse primer from the 3′ fragment. All PCR amplifications were performed for 30 cycles with 1 min of denaturation at 94°C, 1 min of annealing at 52°C, and either 1.5 min (first-round SOE) or 2.25 min (second-round SOE) extension at 72°C. The final product was digested with *Bsi*WI/*Bam*HI and ligated into a similarly digested pC1PCPC2 (42) plasmid. This construct was then digested with *Bam*HI/*Xho*I and the fragment carrying the analytical PCP mutant was ligated into a similarly digested pVibF (35) plasmid. DNA sequencing to verify PCR fidelity was performed on double-stranded DNA by the Molecular Biology Core Facilities of the Dana Farber Cancer Institute (Boston, MA). Constructs for wild-type VibF (35) and the A domain mutant A* of VibF (33) were obtained as previously described.

The described expression plasmids were transformed into *Escherichia coli* BL21 (DE3) competent cells and grown at 15°C in Luria-Bertani media supplemented with 5 mM $MgCl_2$ and 40 μg/mL kanamycin to an OD_{600} of 0.5–0.8 when the culture was induced with 100 μM IPTG and then grown for an additional 12–36 h continuing at 15°C. The cells were harvested by centrifugation at 4000 × *g* for 16 min and stored as pellets at −80°C until further use. Cell pellets from 24 L of culture were thawed and resuspended in 120 mL of lysis buffer (25 mM Tris, pH 8.0, 500 mM NaCl) and then lysed with two passes on an Emulsiflex-C5 cell disruptor (Avestin, Ottawa, Canada). The lysate was cleared by ultracentrifugation at 95000 × *g* for 35 min and then transferred to 3 mL of Ni-NTA Superflow resin (Qiagen, Valencia, CA) for incubation at 4°C for 1.5 h. The resin was then transferred to a column and the protein was eluted with an imidazole gradient using steps of 35 mL of 0 and 5 mM imidazole, 25 mL of 25-mM imidazole, and then 15 mL of 50-, 75-, 100-, 125-, 150-, and 200-mM imidazole mixed into lysis buffer. After running an SDS-PAGE gel to verify which fractions contained the protein, the 100- through 200-mM imidazole fractions were dialyzed overnight against 20 mM Tris, pH 8.0, 50 mM NaCl, 2 mM $MgCl_2$, 1 mM DTT, and 10% glycerol. The dialyzed protein was then concentrated to 3 mL, flash frozen in liquid nitrogen, and stored at −80°C.

Secondary aminoacylation assay

VibB and VibF were initially phosphopantetheinylated with Sfp (44) for 1 h at 30°C in reactions containing 150 mM Tris, pH 7.5, 10 mM $MgCl_2$, 1 mM tris(2-carboxy-ethyl)phosphine hydrochloride (TCEP), 100 μM CoA, 200 μM 2,3-dihydroxybenzoic acid (DHB), 5 μM VibB, 300 nM Sfp, and 250 nM VibF. Secondary aminoacylation was then initiated by the addition of 10 mM ATP, 60 mM Tris, pH 7.5, 1 μM VibE, 50 μM DHP-mOx-NSPD-DHB (prepared as previously described (36)), and 10 mM L-Thr. Reactions were quenched at given time points by addition of nine volumes ice cold methanol and the protein precipitate was removed by centrifugation at 11,600 × *g* for

15 min at 4°C. The resultant supernatant was dried under vacuum and resuspended in 80 μL of 15% acetonitrile. Samples were injected onto a C18 Vydac (Hesperia, CA) smallpore column on a Beckman (Fullerton, CA) System Gold and products were eluted at 1 mL/min in a gradient from 10% to 100% acetonitrile in 0.1% TFA over 23 min. Product elution was monitored at 254 nm. Peak integrations were converted to nanomoles of vibriobactin as described previously (35).

Incubations for L-Thr loading of VibF

Before substrate loading, the PCP domain of VibF (4 μM) was first phosphopantetheinylated in 50 mM Tris, pH 7.0, 5 mM $MgCl_2$, 5 mM TCEP, with 500 nM Sfp and 65 μM CoA-SH for 1–4 h at 30°C in 90-μL reactions. For the A* and PCP_a control experiments, 10 mM L-Thr and 10 mM ATP were added to A* or PCP_a following Sfp treatment in a 100-μL final volume, incubated at 30°C for 15 min, and digested using the protocol described below.

The characteristic time for VibF dimer exchange ranges from 15 min to 1 h (33). For the heterodimer formation and *in trans* activity assays, A* and PCP_a were mixed 1:1 during phosphopantetheinylation (4 h) to allow dimer reequilibration to homodimers and heterodimers. The dimer mixture was then incubated with 10 mM L-Thr and 10 mM ATP for 15 min at 30°C and immediately digested using the protocol described below. For the PCP_a and wild-type VibF time courses, holo-PCP_a or holo-VibF was incubated with 10 mM L-Thr and 10 mM ATP and quenched in 1–5% formic acid at various time points using a KinTek (Austin, TX) quench-flow instrument. For the extreme A*/PCP_a ratio mixing experiments, mixtures of A* and PCP_a were mixed in 1:8 or 8:1 ratios during the phosphopantetheinylation reaction (1 h). The dimer mixture was then incubated with 10 mM L-Thr and 10 mM ATP and quenched in 1–5% formic acid at various time points using a KinTek quench-flow instrument. For all samples quenched by the KinTek quench flow, the pH was readjusted to ~8 before immediate digestion using the protocol described below. Neither enzyme activity nor significant hydrolysis was observed during the digestion process (data not shown).

Digestion conditions

Proteolysis was performed by the addition of *N*-tosyl-L-phenylalanine-chloromethyl ketone-treated trypsin (Promega, Madison, WI) to 0.4 nmol of the target protein at protease/substrate ratios ranging from 1:5 to 1:10 w/w in 50 mM NH_4HCO_3, pH 7.8, and incubated at 30°C for 5 min. Reactions were quenched by the addition of a minimal volume of 10% formic acid (Acros, Morris Plains, NJ) and applied to a wide-pore Jupiter C4 reverse-phase column (Phenomenex, Torrance, CA) with a linear gradient from 10% to 90% MeCN (0.1% TFA) for fractionation. Samples were lyophilized, resuspended in 0.1% trifluoroacetic acid (TFA), desalted via C18-ZipTip (Millipore, Billerica, MA), and eluted in electrospray ionization (ESI) buffer (49% H_2O, 49% MeOH, 2% formic acid) for MS analysis.

ESI/Q-FT and Q-TOF mass spectrometry

ESI was used with a custom quadrupole Fourier-transform (FT) mass spectrometer operating at 8.5 tesla (45) and a micromass quadrupole time-of-flight (Q-TOF) Ultima instrument (Waters, Milford, MA). For FTMS, the ions were directed through a heated metal capillary, skimmer, quadrupole, and multiple ion guides into the ion cell ($\sim 10^{-9}$ Torr) of the FTMS. Scans were acquired at a rate of 1 s^{-1} and data were stored with a MIDAS datastation (46) as 512 K data sets. Spectra were calibrated externally using bovine ubiquitin (M_r = 8559.62 Da) and theoretical isotopic distributions were generated using Isopro v3.0 and fit to experimental data by least squares to assign the most abundant peak. For Q-Tof analysis, samples were introduced through loop injection, the quadrupole operated as an ion guide in MS mode, and a reflectron TOF analyzer placed orthogonally to the quadrupole served as a mass resolving device. The instrument was controlled using MassLynx v4.0 software.

Reported masses and intermediate quantification

High-resolution mass spectrometry of large molecules results in isotopic distributions within the mass spectra, explanations of which have been described previously (47,48). Briefly, all molecular weights in this manuscript are reported as monoisotopic values, which refer to the molecular ion peak composed of the most abundant isotopes of the elements including the mass defect (i.e., C = 12.000000, N = 14.00307, etc.). Assignment of isotopic distributions to the corresponding enzyme intermediates (as displayed in Fig. 4) involved correlating the experimental monoisotopic molecular weights to the theoretical monoisotopic molecular weights for the enzyme intermediates, with a maximum error tolerance of 15 ppm. Two effects disperse MS signals of differentially modified forms of carrier peptides: 1), fractionation of chemically distinct species during chromatography; and 2), multiple charge states observed in ESI-MS. To account for this dispersion, high-performance liquid chromatography (HPLC) fractions (typically two to three) containing different forms of the same carrier peptide are physically mixed before ESI/FTMS analysis and abundance/area information from every charge state observed of a particular species in the broadband spectrum is considered in the determination of relative ratios. The data displayed in Fig. 4 indicate the mass-shifting region of one particular charge state, whereas the relative ratio information reported for a particular experiment has accounted for every charge state present in the mass spectrum. A more detailed explanation and further evaluation of this quantification process has been discussed previously (49,50).

Pre-steady-state kinetic equations and data fitting

Homodimeric VibF contains two A domains, one per VibF chain. Each A domain has the capacity to load L-Thr onto either holo-PCP domain, in an intra- or interchain fashion (33). The probability that a given PCP domain is loaded in an intra- or interchain manner is given by $(1 - P_{inter})$ and P_{inter}, respectively. The associated rates of loading are given by k_{intra} and k_{inter}. In both the PCP_a and wild-type VibF homodimer pre-steady-state A domain experiments, it is observed that the fractions of L-Thr loaded PCP_a and PCP do not approach 100%, but rather saturate around 50% (Fig. 5, *A* and *B*). One explanation for this is that subsets of PCP_a and PCP domains are catalytically incompetent for L-Thr loading. The ratio of competent to incompetent PCP_a domains is given by $\delta[PCP_{a,competent}] = [PCP_{a,incompetent}]$. The proportion of competent PCP_a is then given by $[PCP_{a,competent}]/[PCP_{a,total}] = 1/(1 + \delta)$. Utilizing the same parameter δ, we have the analogous relations for the PCP domains, namely $\delta[PCP_{competent}] = [PCP_{incompetent}]$ and $[PCP_{competent}]/[PCP_{total}] = 1/(1 + \delta)$.

In the A*PCP + PCP_a mixing experiments, the ratio of A*PCP to PCP_a is given by α[A*PCP] = [PCP_a]. Previous biochemical and biophysical experiments have shown that the C1 domain is largely responsible for the dimerization of VibF, and that neither the deletion of the PCP and C2 domains, nor catalytically inactivating point mutations made to the Cy2, PCP, or C2 domains significantly affects the monomer-dimer equilibrium of VibF (33,42). It is assumed, therefore, that the homo- and heterodissociation constants for A*PCP and PCP_a are equivalent. It can then be shown that the proportions of PCP and PCP_a domains in a heterodimer context are given by $[A*PCP{\cdot}PCP_a]/[PCP_{total}] = \alpha/(1 + \alpha)$ and $[A*PCP{\cdot}PCP_a]/[PCP_{a,total}] = 1/(1 + \alpha)$. Note that in the instance of A*PCP·PCP_a heterodimer, there is only one functional copy of the A domain (on the PCP_a chain), and therefore the PCP and PCP_a domains are forced to utilize inter- and intrachain A domain pathways, respectively.

For the PCP_a and wild-type VibF homodimer experiments, the temporal evolution of the fraction of holo-$PCP_{(a)}$ is given by

$$\phi^{PCP_{(a)}}_{holo-PCP_{(a)}}(t) = \frac{1}{(1+\delta)}[P_{inter}e^{-t/k^{-1}_{inter}} + (1 - P_{inter})e^{-t/k^{-1}_{intra}} + \delta],$$

where $\phi^{PCP_{(a)}}_{holo-PCP_{(a)}}$ is the residual fraction of holo-$PCP_{(a)}$ as a function of time, t, after the A domain loading reaction has been initiated with L-Thr.

For the A*PCP + PCP_a mixing experiments, the fractions of holo-PCP_a and holo-PCP are given by

$$\phi_{\text{holo}-\text{PCP}_a}^{\text{A}^*\text{PCP}+\text{PCP}_a}(t) = \frac{1}{(1+\delta)(1+\alpha)} \times [\alpha(P_{\text{inter}}e^{-t/k_{\text{inter}}^{-1}} + (1-P_{\text{inter}})e^{-t/k_{\text{intra}}^{-1}}) + e^{-t/k_{\text{intra}}^{-1}} + \delta(1+\alpha)]$$

$$\phi_{\text{holo}-\text{PCP}}^{\text{A}^*\text{PCP}+\text{PCP}_a}(t) = \frac{1}{(1+\delta)(1+\alpha)}[1 + \alpha e^{-t/k_{\text{inter}}^{-1}} + \delta(1+\alpha)]$$

,

where $\phi_{\text{holo}-\text{PCP}_a}^{\text{A}^*\text{PCP}+\text{PCP}_a}$ and $\phi_{\text{holo}-\text{PCP}}^{\text{A}^*\text{PCP}+\text{PCP}_a}$ are the residual fractions of holo-PCP_a and holo-PCP, respectively. Note that in the expressions above, we must account for the two subpopulations of $PCP_{(a)}$: one is in the context of the heterodimer, and the other is in the context of the homodimer.

The system of equations for the pre-steady-state VibF A domain kinetics model presented above contains four free parameters, namely δ, P_{inter}, k_{inter}, and k_{intra}. These parameters were fit to the observed experimental data by the numerical optimization method of steepest descent, minimizing the sum of the residual errors squared. The R value given in Table 1 is Pearson's correlation coefficient. Gaussian noise comparable to that characteristic of the experimental technique ($\mu = 0\%$, $\sigma = 5\%$) was applied to the observed data, and pseudo-best-fit parameters were derived by refitting to the perturbed data. This procedure was repeated ($N = 10{,}000$) times to generate a distribution of pseudo-best-fit parameters, and these were then utilized to estimate the error in the best-fit parameters, providing the mean, standard deviation, and 95% confidence intervals for each parameter derived directly from the pseudo-best-fit distributions. The data fitting and best-fit parameter error estimation programs are available from the authors upon request.

To estimate the average fraction of secondary aminoacylation cycle time attributable to L-Thr acylation, we divide the average acylation time by the total cycle time, which is simply the inverse of the experimentally determined secondary aminoacylation rate. The average time required to perform L-Thr acylation, in terms of the best-fit kinetic parameters, is given by $(1 - P_{\text{inter}})/k_{\text{intra}} + P_{\text{inter}}/k_{\text{inter}}$.

RESULTS

Generation and secondary aminoacylation assay of the analytical mass mutant PCP_a

To discriminate intra- from interchain acylation of the VibF PCP domain following L-Thr adenylation, we exploit the fact that in heterodimers of wild-type and inactive A domain mutants of VibF, the PCP domain *in cis* to the active A domain can only undergo intrachain catalysis and the PCP domain *in trans* to the active A domain can only undergo interchain catalysis (Fig. 2). A consequence of proteolytic processing that is requisite before MS identification of intermediates bound to the phosphopantetheinylated serine active site of the PCP domain (see Experimental Procedures) is the loss of topological information linking a given PCP domain *in cis* with an active or mutated A domain. To preserve this information after proteolysis, an analytical mass mutant of VibF was generated to differentiate the PCP domains that lie *in cis* to an active A domain.

TABLE 1 Best-fit parameters from numerical modeling of VibF adenylation activity in the pre-steady-state

		Pseudo-best-fit parameter distribution ($N = 10{,}000$)	
Free parameter	Best fit	Mean ± SD	95% Confidence interval
δ	1.0	1.0 ± 0.1	0.8–1.3
P_{inter} (%)	52	51 ± 11	32–68
k_{inter} (s^{-1})	3.0	3.3 ± 0.6	2.4–4.4
k_{intra} (s^{-1})	44	41 ± 9	17–51
R	0.90		

Five residues downstream from the phosphopantetheinylated Ser^{1891} in VibF lies Arg^{1896}, which is closely followed by Arg^{1900}. Replacing Arg^{1896} with Thr (R1896T), a mutation predicted to be well tolerated on the basis of sequence alignment to other known PCP domains (data not shown), results in a PCP_a mutant that after trypsinolysis yields a peptide fragment containing Ser^{1891}, spanning from Ser^{1871} to Arg^{1900} (3126.50 Da) that is 370.22 Da larger than the analogous fragment derived from the wild-type PCP domain, spanning from Ser^{1871} to Arg^{1896} (2756.28 Da) (Fig. 2). Even after heterodimers of the VibF analytical mass mutant PCP_a and the inactive A domain mutant A* (containing a wild-type PCP domain) have been digested with trypsin, it remains discernible which PCP fragments underwent interchain catalysis, namely the smaller wild-type proteolytic fragments derived from A*, and which underwent intrachain catalysis, namely the larger analytical mutant proteolytic fragments derived from PCP_a (schematized in Fig. 2).

The analytical mutant was generated using standard PCR and molecular biology techniques described in Experimental Procedures. All VibF constructs, wild-type, A*, and PCP_a, were expressed in *E. coli* as C-terminal His-tagged proteins and purified by nickel affinity chromatography. All proteins were obtained in comparable yield (1–2 mg/L) and purity (95%), and migration on SDS-12% PAGE was consistent with the calculated VibF mass of 271 kDa (Supplementary Material, Fig. S1).

Once the analytical mass mutant was generated, it was tested against wild-type VibF enzyme for its ability to catalyze secondary aminoacylation. In this assay, VibF must generate (dihydroxyphenyl)methyloxazolinyl-*S*-VibF (DHP-mOx-*S*-VibF) before the transfer of this species to the N_5 of the DHP-mOx-norspermidine-dihydroxybenzoyl (DHP-mOx-NSPD-DHB) intermediate substrate to form the final vibriobactin product (Fig. 1) (36). Using initial rates of vibriobactin production, it was determined that the secondary aminoacylation k_{cat} for the analytical mass mutant (8.2 ± 0.3 min^{-1}) was ~3.6 times slower than that for wild-type VibF (29 ± 0.7 min^{-1}). Although the analytical mutant was designed to be minimally perturbative to the function of VibF, it does appear to modestly alter the kinetics of vibriobactin production. However, this finding does not affect the conclusions of this study, because all subsequent interrogation of intra versus inter catalytic rates was focused on the A domain and its initial loading of L-Thr onto VibF. Vibriobactin production, as assayed by secondary aminoacylation, requires

a subsequent sequence of catalytic activities, and it is probable that the analytical mass mutation does not affect A domain function but rather perturbs a subsequent condensation/heterocyclization processing step.

Identification of active-site Ser^{1891}-containing peptides

Exhaustive trypsin digestion of apo-A* yielded a 2756.31-Da peptide (Fig. 3 A) in HPLC fraction 24, which matched within 15 ppm to the PCP active site containing peptide S_{1871}–R_{1896} ($M_{theoretical}$ = 2756.28 Da). Correlation of subsequent tandem MS (MS/MS) fragmentation data (Fig. 3 *B*), produced via collisionally activated dissociation, to the peptide primary sequence validated the identity of the active site containing peptide (Fig. 3 *C*). Analogously, a trypsin digest of the apo-PCP_a yielded a 3126.52 Da peptide in HPLC fraction 25, which matched within 15 ppm to S^{1871}–R^{1900} ($M_{theoretical}$ = 3126.50 Da). Subsequent MS/MS also validated the identity of this active site containing peptide (data not shown). Examination of every individual HPLC fraction yielded no detectable incompletely digested active site containing peptides.

Adenylation mutant A* and analytical mass mutant PCP_a control experiments

Incubation of the A* and PCP_a constructs with Sfp (44) and coenzyme A resulted in nearly complete phosphopantetheinylation of their respective PCP active sites to the holo- form (+340 Da), as seen in Fig. 4, *A* and *C*, respectively, with no trace of apo- enzyme detectable. Subsequent incubation of the holo-A* construct with the natural A domain substrate L-Thr yielded no detectable loading onto the PCP active site (Fig. 4 *B*), as expected since the adenylation activity has been abrogated with the D1092A mutation (33). However, incubation of holo-PCP_a with L-Thr resulted in a mass shift of +101 Da, corresponding to the holo- form of the protein that had become self-loaded with L-Thr (Fig. 4 *D*).

Validation of heterodimer formation and interchain L-Thr acylation

Although it has been previously shown that FAS and PKS dimers may be dissociated and reassociated by altering salt concentrations, temperature, or utilization of anion-exchange chromatography (24,51), VibF dimers spontaneously separate into monomers and reassociate under enzymatic assay conditions (33). Incubation of a preequilibrated 1:1 mixture of holo-A* and holo-PCP_a with L-Thr for 15 min resulted in L-Thr loading of the PCP domain of A* (Fig. 4 *E*), confirming both formation of heterodimeric species under the assay conditions and the interchain transfer of L-Thr across the dimer, as was shown previously by in vitro mutant complementation assays (33). This key result validates this experimental approach, as is schematized in Fig. 2.

Pre-steady-state L-Thr acylation time courses and data fitting

To ensure that A domain activation and loading of L-Thr onto the VibF PCP domain was unaffected by the analytical mass mutation PCP_a, pre-steady-state loading assays were performed for both wild-type and PCP_a VibF. In these assays, the PCP_a mass mutant performed comparably to wild-type VibF (Fig. 5, *A* and *B*), indicating that the reduction in k_{cat} observed for overall vibriobactin production in the analytical mutant must be a consequence of a subsequent processing step. Then, pre-steady-state loading assays were performed on mixtures of homodimers and heterodimers (Fig. 5, *C* and *D*). To minimize the background signal from homodimers (A*·A* and PCP_a·PCP_a) present in

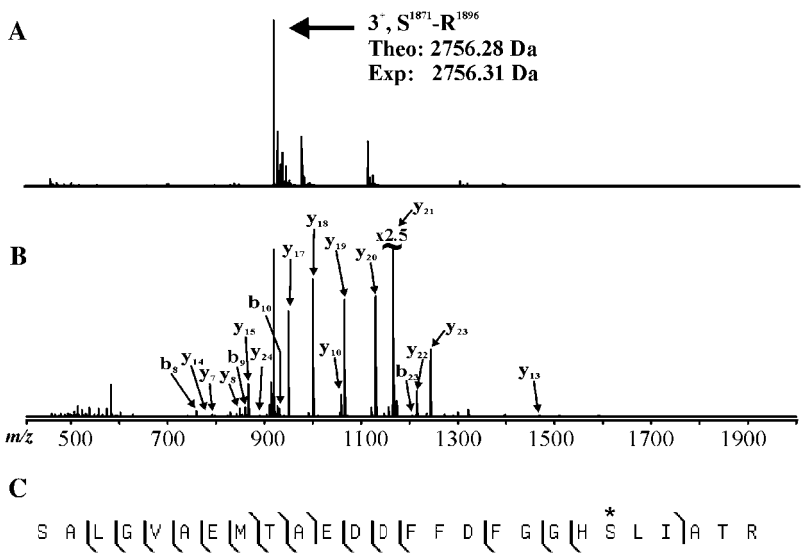

FIGURE 3 Identification of the proteolytic fragment containing the active site serine of VibF-PCP. (*A*) Fourier-transform mass spectrum (25 scans) of fraction 24 of a tryptic digest of apo-A*; the most abundant species observed corresponds to the 3+ charge state of the proteolytic fragment Ser^{1871}–Arg^{1896} (experimental M_r = 2756.31 Da), which contains the VibF-PCP active site serine (Ser^{1891}). (*B*) Subsequent MS/MS fragmentation and verification of the 2.7 kDa species assignment observed in *A* after signal enhancement through selected ion accumulation using the quadrupole Fourier-transform mass spectrometer; fragment ions are described by which terminus they contain (i.e., *b* ions contain the N-terminus and *y* ions the C terminus), and the *y* axis has been expanded by a factor of 2.5 to aptly visualize the fragment ions. Fragment ions labeled range in charge state from 1+ to 3+. (*C*) Fragment ion map correlating the ions observed in *B* to the sequence of the PCP carrier peptide (Ser^{1871}–Arg^{1896}) generated from trypsinolysis of apo-A*. Asterisk indicates active-site Ser^{1891}.

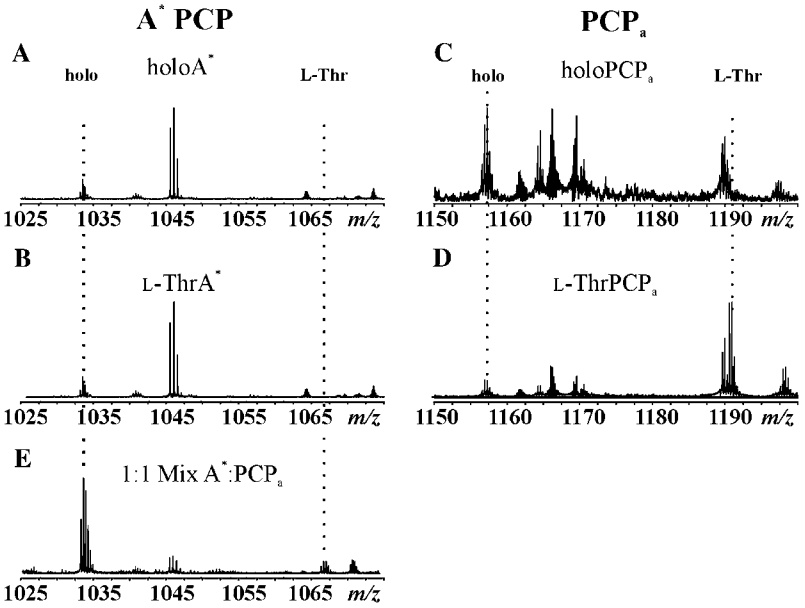

FIGURE 4 A*, PCP_a, and heterodimer formation control experiments. The mass shifting regions for the 3+ ions of the A*PCP domain for the (*A*) holo experiment and (*B*) L-Thr loading experiment (1025–1075 *m/z*), and for the 3+ ions of the PCP_a domain for the (*C*) holo experiment and (*D*) L-Thr loading experiment (1150–1200 *m/z*). The results for each experiment confirmed expectations: the A* construct was unable to load L-Thr, whereas the PCP_a construct was active in L-Thr acylation. (*E*) Validation of heterodimer formation and interchain L-Thr acylation. A 1:1 mixture of A* and PCP_a yielded heterodimer formation and subsequent L-Thr acylation on the A*PCP domain, as displayed in the mass shifting region (1025–1075 *m/z*) for the 3+ ions of A*PCP.

solution, mixtures of A* and PCP_a were combined in 1:8 and 8:1 ratios for the formation of heterodimers (A*·PCP_a). The idea here is to use relatively trace amounts of A* or PCP_a, so that the background is minimized while still providing enough A*·PCP_a signal. At an 8:1 ratio of A*/PCP_a, 8/9 of PCP_a is in the context of heterodimer, which means that only 1/9 of PCP_a is homodimer background. The ratio selected was optimized for detection with this MS-based assay and could not be increased beyond 8:1 because then the total amount of PCP_a becomes too small to detect. Given the small size of the PCP-containing peptide, the resolution of ~10,000 from a Q-TOF instrument was sufficient for the majority of kinetic time points acquired here.

Given the results from the pre-steady-state experiments, we developed a minimal mechanistic model for VibF L-Thr acylation that was consistent with the data. The model is shown in Fig. 6, and the details of its mathematical implementation are described in Experimental Procedures. The essence of the model is that there are probabilities for a given PCP domain to be loaded in an intrachain fashion $(1 - P_{\text{inter}})$

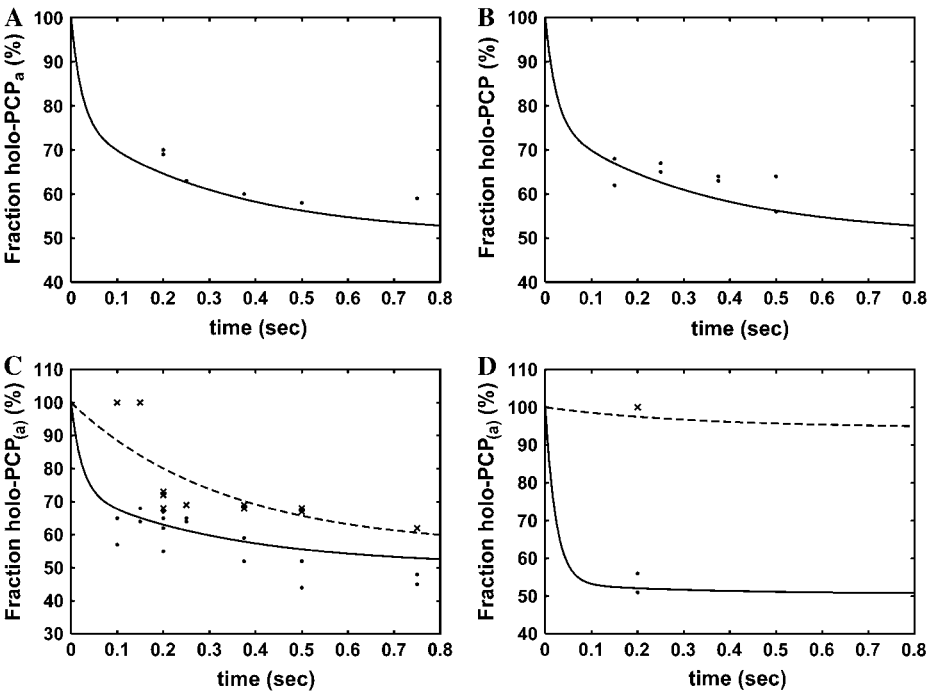

FIGURE 5 Time courses of holo-$PCP_{(a)}$ loading. Homodimer experiments: (*A*) PCP_a, eight data points, and (*B*) wild-type VibF, six data points. A*PCP + PCP_a mixing experiments: (*C*) A*PCP/PCP_a = 1:8, 32 data points, and (*D*) A*PCP/PCP_a = 8:1, four data points. Observed data shown as data points (*dots*, PCP_a; *cross-hatching*, PCP). Pre-steady-state kinetics model shown as lines (*solid line*, PCP_a; *dashed line*, PCP). Some data points are overlapping (see supplemental data Table S1).

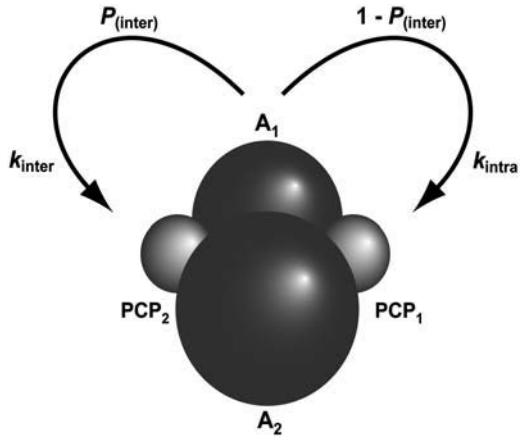

FIGURE 6 Model for VibF A domain kinetics. Hypothetical placement of A and PCP domains within homodimeric VibF (Cy1, Cy2, C1, and C2 domains removed for clarity). Subscript numbering assigns each domain to one of the two VibF chains. Each PCP domain may be loaded by an A domain in an intra- or interchain fashion, with associated probabilities $(1 - P_{inter})$ and P_{inter}, and rates k_{intra} and k_{inter}, respectively.

or in an interchain fashion (P_{inter}), and there are acylation rates associated with each pathway, namely k_{intra} and k_{inter}, respectively. There is only one additional free parameter in the model, δ, which dictates the fraction of $PCP_{(a)}$ that is unable to be loaded. The benefits of this particular model are that it contains only four free parameters, yet is sufficient to describe the L-Thr acylation flux, and the characteristic intra- and interchain loading rates. The results of fitting the model's parameters to the data are given in Table 1. Notably, the probability for a given PCP domain to be loaded in an interchain fashion (P_{inter}) is not significantly different from 50% (consistent with a neutral flux for L-Thr loading), and the best-fit intrachain loading rate (k_{intra}) is significantly faster than the interchain rate (k_{inter}).

DISCUSSION

Despite biochemical characterization of VibF, fundamental questions concerning rates of catalysis of individual domains remained unresolved. Previous steady-state heterodimeric mutant complementation experiments established that the Cy1, Cy2, and A catalytic domains within VibF act on tethered intermediates in both intra- and interchain fashions, whereas C2 appears to operate predominantly in an intrachain manner (33). However, the actual kinetic preference for intra- or interchain catalysis would be masked if both occur faster than the rate-limiting step. The strategy described herein enables the determination of pre-steady-state intra- versus interchain rates and flux preferences for non-rate-limiting steps in a competitive context (i.e., both pathways are possible and in competition with each other), in contrast with previous complementation experiments in which only one pathway was possible.

Here, a mass spectrometric approach has been used to monitor enzymatic activities resulting from mixtures of the A* (catalytically inactive A domain mutant) and PCP_a (analytical mass mutant) constructs to determine the pre-steady-state rates of VibF intra- and interchain acylation and to what extent L-Thr is transferred through each pathway. Essential for the MS-based approach described here, the catalytically active analytical mass mutant construct was introduced to distinguish the two carrier protein domains (PCP and PCP_a) involved in the dimeric complex by a mass difference after proteolysis. Indeed, the exploration of covalent catalysis, exploitation of high mass accuracy, and the ability to obtain semiquantifiable regiospecific information warrants futher refinement and application of this strategy to other such systems containing higher-order quaternary structure. For example, the extension of this strategy to other dimeric FAS and PKS multienzyme complexes, for which nearly pure heterodimers can be isolated by dual-affinity chromatography of differentially tagged constructs (27), would allow for the examination of flux partitioning in a competitive context while simultaneously simplifying the modeling necessary (as the active homodimer background would be absent from the experiment).

The benefits of the mass spectrometric approach developed in this work merit comparison with what more conventional rapid-quench approaches provide. A traditional route would be to perform the complementation assay at pre-steady-state with a radio-labeled substrate in a rapid-quench device, working up the reaction with hydrolysis and subsequent quantitation of the intermediate via radioactive chromatography (52,53). Unlike the MS approach, which utilizes an analytical mass mutation (PCP_a) to directly determine the product attributable to each pathway, the traditional rapid-quench approach cannot distinguish between product fractions arising from intra- and interchain pathways. A consequence is that traditional rapid-quench requires the use of specific complementation pairs for which only one pathway is possible (e.g., only the interchain pathway is permitted in heterodimers of A* and PCP*). Although these prerequisite pair selections can result in determinations of k_{intra} and k_{inter}, the rates are not entirely physiologically relevant, because they are not measured when the two pathways are in competition with each other. In contrast, the MS approach uses complementation pairs for which both pathways are possible (e.g., in heterodimers of A* and PCP_a), and thereby does not suffer from this limitation. Another concern with the traditional approach is that it requires normalization of the product output, and thus is dependent on accurate estimates for the total enzyme concentration, as well as for the ratio of concentrations for the two mutant proteins in the complementation pair. There is no normalization required for the MS approach, which measures the intermediate while still attached to the PCP peptide fragment.

When determining the secondary aminoacylation rate for wild-type VibF, the measured k_{cat} was found to be 29 ±

0.7 min^{-1}, which is different from the previously published rates of 41 min^{-1} (36) and 48 min^{-1} (33,42). These differences are attributed to slight protocol variations in VibF protein preparation between this work and previous studies, as the k_{cat} values reported here were reproducible with separate batch preparations of VibF (data not shown). Furthermore, it was unanticipated that the analytical mass mutation PCP_a would result in a 3.6-fold reduction in the secondary aminoacylation rate relative to wild-type VibF. Since many PCP domains have a threonine at the position of the VibF PCP_a R1896T substitution, we speculate that it is not threonine itself, but possibly threonine in the context of spatially neighboring VibF residues, that is responsible for this reduction in aminoacylation rate. Subsequent pre-steady-state L-Thr acylation experiments revealed that the mutation minimally affected the A domain (Fig. 5, *A* and *B*), and therefore must affect some subsequent catalytic step in vibriobactin formation. However, despite determining that the overall rate of acylation is unaffected, we are unable to unambiguously show that the analytical mass mutation does not perturb the flux across the heterodimer. It is interesting to note that this single point mutation in a nonconserved surface-exposed residue could cause such a noticeable effect and argues that individual residues within the PCP domain may be important to some, but not necessarily all, interactions with upstream and downstream domains.

There are several features of the pre-steady state experimental data that should be highlighted. L-Thr loading saturates near 50% for both PCP_a and wild-type VibF (Fig. 5, *A* and *B*, and Supplementary Material, Table S1). Because this observation is common to both PCP_a and wild-type VibF, the analytical mass mutation PCP_a is not implicated as the cause, but the effect could be explained by subpopulations of $PCP_{(a)}$ (referring to PCP and/or PCP_a) that are unable to be successfully loaded (at least on the time scale of the assay), a competition between loading and hydrolysis, subpopulations of PCP_a and wild-type VibF with inoperable A domains, or various combinations thereof. It should be pointed out that it is not possible with the current data to discriminate between these hypotheses. Incorporation of hydrolysis and/or inoperable A domains into the model would result in very similar estimates for P_{inter} and k_{intra}:k_{inter}, but would tend to increase the absolute fitted values of k_{intra} and k_{inter}.

As can be surmised from the spread in the replicate data points shown in Fig. 5 and listed in supplemental Table S1, the standard measurement error of the fraction of holo-$PCP_{(a)}$ is in the neighborhood of $\pm 5\%$, but the absolute error is likely to be more extreme when the L-Thr-*S*-$PCP_{(a)}$ species is not very abundant. In the 1:8 A*/PCP_a mixing experiment, loaded PCP is not observed for the first two time points (0.10 and 0.15 s). It seems unlikely that there is no loading until 0.20 s, at which point $\sim$30% of the PCPs are observed to be loaded. A reasonable explanation for the first two time points is that there is simply not enough signal to detect the loaded PCP species. In this particular mixing experiment, only 1/9 of the total protein is A*, and thus there is much less total signal in the PCP channel than in the PCP_a channel.

The correlation coefficient between the pre-steady-state experimental data and the model for A domain function is modest at $R = 0.90$. The above noted $\pm 5\%$ standard measurement error and the absolute measurement error due to instances of insufficient L-Thr-*S*-$PCP_{(a)}$ signal both contribute to the data fitting error. It would be possible to improve the data fitting with additional free parameters (such as a distinct δ for each preparation of PCP_a, A*, and wild-type VibF), but this would lead to concerns of over-fitting the data and would not provide any additional mechanistic insight.

The best-fit P_{inter} value of 52% is consistent with a neutral L-Thr flux. The 95% confidence interval for P_{inter} between 32% and 68% is tighter than would be expected for a uniformly random distribution, but does not provide ample assurance that the flux is not skewed moderately toward the intra- or interchain pathways. On the other hand, the best-fit intrachain loading rate (k_{intra}) is significantly faster than the interchain rate (k_{inter}), with 95% confidence that k_{intra} is at least 14 s^{-1} faster than k_{inter}, and none of the $N = 10{,}000$ pseudo data-fittings resulted in $k_{inter} > k_{intra}$.

Attempts to identify thioester bound intermediates on VibF during steady state, and thus to determine the rate-limiting step in vibriobactin production, were unsuccessful due to two major difficulties. In addition to VibF and Sfp, which are present in L-Thr acylation assays, VibB, VibE, and VibH are required to reconstitute steady-state vibriobactin production (Fig. 1). We were unable to unambiguously identify intermediate-bound VibF PCP fragments after trypsinolysis by MS due to the presence of many other coeluting fragments of similar mass derived from VibB, VibE, and/or VibH. Therefore, we could not identify the intermediates as enzyme-tethered species. Additionally, the methyl-oxazaline ring in the DHP-mOx-*S*-PCP intermediate is extremely labile and readily reforms the DHB-L-Thr-*S*-PCP intermediate under both acidic and basic conditions, which would yield incorrect proportions of intermediate partitioning. Thus, we could not cleave the intermediates off of the enzyme and identify them as soluble species.

The best-fit kinetic parameters derived from the pre-steady-state L-Thr acylation experiments are consistent with previous in vitro mutant complementation results for VibF. As determined by the best-fit values for the pre-steady-state kinetics (see Experimental Procedures), L-Thr acylation should account for $\sim$9% of the secondary aminoacylation cycle time. With four intermediates partitioned on VibF during steady state, this projection implies that L-Thr acylation is not the rate-limiting step in vibriobactin formation. In previous complementation experiments, the VibF mutant pair with the active A domain located *in cis* to the active PCP domain (i.e., utilizing intrachain A domain activity), produced vibriobactin more quickly than those pairs with the

active A domain operating in an interchain fashion (33). This is in agreement with the best-fit k_{intra} being significantly faster than k_{inter}, given that the A domain activity is not the rate-limiting step.

We have developed a probabilistic kinetic model coupled with a mass spectrometric approach to probe intra- and interchain rates and corresponding fluxes of catalytic steps performed within dimeric NRPS, FAS, and PKS enzyme complexes, demonstrating proof of principle through the application of the methodology to VibF, an NRPS subunit of vibriobactin synthetase. The higher-order oligomeric structural arrangements of NRPSs, FASs, and PKSs allow for alternate paths of product elongation, as the cascade of intermediates can flow in *cis* (intrachain) or *trans* (interchain) along the enzymatic assembly line. Although previous steady-state complementation studies have been able to establish which catalytic steps may operate in intra- and/or interchain fashions, this has been in the context of only one pathway being available at a time. The approach we forward here utilizes rapid-quench experiments coupled with a reporter mutation and mass spectrometry to distinguish pre-steady-state intra- versus interchain rates and flux preferences for non-rate-limiting steps in a competitive context (i.e., both pathways are possible and in competition with each other). The analytical mass mutant concept may be applied fruitfully to a diversity of tasks beyond NRPS, FAS, and PKS characterization, especially when it is desirable to distinguish peptide digest fragments originating from highly homologous proteins. A sample application would be to facilitate the mass spectrometric determination of protein complex topology via cross-linking and subsequent digest, when multiple subunits within the complex have very high sequence identity.

SUPPLEMENTARY MATERIAL

An online supplement to this article can be found by visiting BJ Online at http://www.biophysj.org.

We thank Michael Boyne and Frédéric Vaillancourt for reading of the manuscript, and Furong Sun and Richard Milberg for assistance in collecting data with the Q-TOF Ultima mass spectrometer, which was purchased in part with a grant from the National Science Foundation, Division of Biological Infrastructure (DBI-0100085).

This work was supported by grants from the National Institutes of Health (GM 067725 to N.L.K., GM 20011 to C.T.W). N.J.H. is a Damon Runyon Fellow supported by the Damon Runyon Cancer Research Foundation (DRG-1880-05). We further acknowledge generous support from the Sloan Foundation, a National Science Foundation Graduate Research Fellowship to L.M.H., a Pharmacological Sciences Training Grant from the National Institute of General Medical Sciences, and an National Defense Science and Engineering Graduate Fellowship to C.J.B.

REFERENCES

1. Cane, D. E., and C. T. Walsh. 1999. The parallel and convergent universes of polyketide synthases and nonribosomal peptide synthetases. *Chem. Biol.* 6:R319–R325.
2. Cane, D. E., C. T. Walsh, and C. Khosla. 1998. Harnessing the biosynthetic code: combinations, permutations, and mutations. *Science.* 282:63–68.
3. Schwarzer, D., and M. A. Marahiel. 2001. Multimodular biocatalysts for natural product assembly. *Naturwissenschaften.* 88:93–101.
4. Weber, T., and M. A. Marahiel. 2001. Exploring the domain structure of modular nonribosomal peptide synthetases. *Structure.* 9:R3–R9.
5. Smith, S., A. Witkowski, and A. K. Joshi. 2003. Structural and functional organization of the animal fatty acid synthase. *Prog. Lipid Res.* 42:289–317.
6. Keating, T. A., and C. T. Walsh. 1999. Initiation, elongation, and termination strategies in polyketide and polypeptide antibiotic biosynthesis. *Curr. Opin. Chem. Biol.* 3:598–606.
7. Conti, E., T. Stachelhaus, M. A. Marahiel, and P. Brick. 1997. Structural basis for the activation of phenylalanine in the nonribosomal biosynthesis of gramicidin S. *EMBO J.* 16:4174–4183.
8. Weber, T., R. Baumgartner, C. Renner, M. A. Marahiel, and T. A. Holak. 2000. Solution structure of PCP, a prototype for the peptidyl carrier domains of modular peptide synthetases. *Struct. Fold. Des.* 8: 407–418.
9. Tsai, S. C., L. J. Miercke, J. Krucinski, R. Gokhale, J. C. Chen, P. G. Foster, D. E. Cane, C. Khosla, and R. M. Stroud. 2001. Crystal structure of the macrocycle-forming thioesterase domain of the erythromycin polyketide synthase: versatility from a unique substrate channel. *Proc. Natl. Acad. Sci. USA.* 98:14808–14813.
10. Keating, T. A., C. G. Marshall, C. T. Walsh, and A. E. Keating. 2002. The structure of VibH represents nonribosomal peptide synthetase condensation, cyclization and epimerization domains. *Nat. Struct. Biol.* 9:522–526.
11. Pan, H., S. Tsai, E. S. Meadows, L. J. Miercke, A. T. Keatinge-Clay, J. O'Connell, C. Khosla, and R. M. Stroud. 2002. Crystal structure of the priming β-ketosynthase from the R1128 polyketide biosynthetic pathway. *Structure.* 10:1559–1568.
12. Watanabe, K., C. Khosla, R. M. Stroud, and S. C. Tsai. 2003. Crystal structure of an Acyl-ACP dehydrogenase from the FK520 polyketide biosynthetic pathway: insights into extender unit biosynthesis. *J. Mol. Biol.* 334:435–444.
13. Li, Q., C. Khosla, J. D. Puglisi, and C. W. Liu. 2003. Solution structure and backbone dynamics of the holo form of the frenolicin acyl carrier protein. *Biochemistry.* 42:4648–4657.
14. Witkowski, A., A. Ghosal, A. K. Joshi, E. Witkowska, F. J. Asturias, and S. Smith. 2004. Head-to-head coiled arrangement of the subunits of the animal fatty acid synthase. *Chem. Biol.* 11:1667–1676.
15. Jenni, S., M. Leibundgut, T. Maier, and N. Ban. 2006. Architecture of a fungal fatty acid synthase at 5 Å resolution. *Science.* 311:1263–1267.
16. Maier, T., S. Jenni, and N. Ban. 2006. Architecture of mammalian fatty acid synthase at 4.5 A resolution. *Science.* 311:1258–1262.
17. Smith, S., and S. Abraham. 1970. Fatty acid synthetase from lactating rat mammary gland. I. Isolation and properties. *J. Biol. Chem.* 245: 3209–3217.
18. Smith, S., and S. Abraham. 1971. Fatty acid synthetase from lactating rat ammary gland. III. Dissociation and reassociation. *J. Biol. Chem.* 246:6428–6435.
19. Wakil, S. J. 1989. Fatty acid synthase, a proficient multifunctional enzyme. *Biochemistry.* 28:4523–4530.
20. Joshi, A. K., and S. Smith. 1993. Construction, expression, and characterization of a mutated animal fatty acid synthase deficient in the dehydrase function. *J. Biol. Chem.* 268:22508–22513.
21. Witkowski, A., A. K. Joshi, V. S. Rangan, A. M. Falick, H. E. Witkowska, and S. Smith. 1999. Dibromopropanone cross-linking of the phosphopantetheine and active-site cysteine thiols of the animal fatty acid synthase can occur both inter- and intrasubunit. *J. Biol. Chem.* 274:11557–11563.
22. Staunton, J., P. Caffrey, J. F. Aparicio, G. A. Roberts, S. S. Bethell, and P. F. Leadlay. 1996. Evidence for a double-helical structure for modular polyketide synthases. *Nat. Struct. Biol.* 3:188–192.

23. Gokhale, R. S., J. Lau, D. E. Cane, and C. Khosla. 1998. Functional orientation of the acyltransferase domain in a module of the erythromycin polyketide synthase. *Biochemistry*. 37:2524–2528.

24. Kao, C. M., R. Pieper, D. E. Cane, and C. Khosla. 1996. Evidence for two catalytically independent clusters of active sites in a functional modular polyketide synthase. *Biochemistry*. 35:12363–12369.

25. Joshi, A. K., A. Witkowski, and S. Smith. 1997. Mapping of functional interactions between domains of the fatty acid synthase by mutant complementation in vitro. *Biochemistry*. 36:2316–2322.

26. Joshi, A. K., A. Witkowski, and S. Smith. 1998. The malonyl/acetyltransferase and β-ketoacyl synthase domains of the animal fatty acid synthase can cooperate with the acyl carrier protein domain of either subunit. *Biochemistry*. 37:2515–2523.

27. Rangan, V. S., A. K. Joshi, and S. Smith. 2001. Mapping the functional topology of the animal fatty acid synthase by mutant complementation in vitro. *Biochemistry*. 40:10792–10799.

28. Joshi, A. K., V. S. Rangan, A. Witkowski, and S. Smith. 2003. Engineering of an active animal fatty acid synthase dimer with only one competent subunit. *Chem. Biol*. 10:169–173.

29. Brink, J., S. J. Ludtke, C. Y. Yang, Z. W. Gu, S. J. Wakil, and W. Chiu. 2002. Quaternary structure of human fatty acid synthase by electron cryomicroscopy. *Proc. Natl. Acad. Sci. USA*. 99:138–143.

30. Brink, J., S. J. Ludtke, Y. Kong, S. J. Wakil, J. Ma, and W. Chiu. 2004. Experimental verification of conformational variation of human fatty acid synthase as predicted by normal mode analysis. *Structure*. 12: 185–191.

31. Ming, D., Y. Kong, M. A. Lambert, Z. Huang, and J. Ma. 2002. How to describe protein motion without amino acid sequence and atomic coordinates. *Proc. Natl. Acad. Sci. USA*. 99:8620–8625.

32. Asturias, F. J., J. Z. Chadick, I. K. Cheung, H. Stark, A. Witkowski, A. K. Joshi, and S. Smith. 2005. Structure and molecular organizaton of mammalian fatty acid synthase. *Nat. Struct. Mol. Biol*. 12:225–232.

33. Hillson, N. J., and C. T. Walsh. 2003. Dimeric structure of the six-domain VibF subunit of vibriobactin synthetase: mutant domain activity regain and ultracentrifugation studies. *Biochemistry*. 42:766–775.

34. Sieber, S. A., U. Linne, N. J. Hillson, E. Roche, C. T. Walsh, and M. A. Marahiel. 2002. Evidence for a monomeric structure of nonribosomal peptide synthetases. *Chem. Biol*. 9:997–1008.

35. Keating, T. A., C. G. Marshall, and C. T. Walsh. 2000. Reconstitution and characterization of the *Vibrio cholerae* vibriobactin synthetase from VibB, VibE, VibF, and VibH. *Biochemistry*. 39:15522–15530.

36. Marshall, C. G., N. J. Hillson, and C. T. Walsh. 2002. Catalytic mapping of the vibriobactin biosynthetic enzyme VibF. *Biochemistry*. 41:244–250.

37. Bevitt, D. J., J. Cortes, S. F. Haydock, and P. F. Leadlay. 1992. 6-Deoxyerythronolide-B synthase 2 from *Saccharopolyspora erythraea*. Cloning of the structural gene, sequence analysis and inferred domain structure of the multifunctional enzyme. *Eur. J. Biochem*. 204:39–49.

38. Ikeda, H., T. Nonomiya, M. Usami, T. Ohta, and S. Omura. 1999. Organization of the biosynthetic gene cluster for the polyketide anthelmintic macrolide avermectin in *Streptomyces avermitilis*. *Proc. Natl. Acad. Sci. USA*. 96:9509–9514.

39. Tang, L., Y. J. Yoon, C. Y. Choi, and C. R. Hutchinson. 1998. Characterization of the enzymatic domains in the modular polyketide synthase involved in rifamycin B biosynthesis by *Amycolatopsis mediterranei*. *Gene*. 216:255–265.

40. Crosa, J. H., and C. T. Walsh. 2002. Genetics and assembly line enzymology of siderophore biosynthesis in bacteria. *Microbiol. Mol. Biol. Rev*. 66:223–249.

41. Du, L., C. Sanchez, M. Chen, D. J. Edwards, and B. Shen. 2000. The biosynthetic gene cluster for the antitumor drug bleomycin from *Streptomyces verticillus* ATCC15003 supporting functional interactions between nonribosomal peptide synthetases and a polyketide synthase. *Chem. Biol*. 7:623–642.

42. Hillson, N. J., C. J. Balibar, and C. T. Walsh. 2004. Catalytically inactive condensation domain C1 is responsible for the dimerization of the VibF subunit of vibriobactin synthetase. *Biochemistry*. 43:11344–11351.

43. Ho, S. N., H. D. Hunt, R. M. Horton, J. K. Pullen, and L. R. Pease. 1989. Site-directed mutagenesis by overlap extension using the polymerase chain reaction. *Gene*. 77:51–59.

44. Quadri, L. E. N., P. H. Weinreb, M. Lei, M. M. Nakano, P. Zuber, and C. T. Walsh. 1998. Characterization of Sfp, a *Bacillus subtilis* phosphopantetheinyl transferase for peptidyl carrier protein domains in peptide synthetases. *Biochemistry*. 37:1585–1595.

45. Patrie, S. M., J. P. Charlebois, D. Whipple, N. L. Kelleher, C. L. Hendrickson, J. P. Quinn, A. G. Marshall, and B. Mukhopadhyay. 2004. Construction of a hybrid quadrupole/Fourier transform ion cyclotron resonance mass spectrometer for versatile MS/MS above 10 kDa. *J. Am. Soc. Mass Spectrom.* 15:1099–1108.

46. Senko, M. W., J. D. Canterbury, S. Guan, and A. G. Marshall. 1996. A high-performance modular data system for Fourier transform ion cyclotron resonance mass spectrometry. *Rapid Commun. Mass Spectrom.* 10:1839–1844.

47. Yergey, J., D. Heller, G. Hansen, R. J. Cotter, and C. Fenselau. 1983. Isotopic distributions in mass spectra of large molecules. *Anal. Chem.* 55:353–356.

48. McLafferty, F. W. 1994. High-resolution tandem FT mass spectrometry above 10 kDa. *Acc. Chem. Res*. 27:379–386.

49. Hicks, L. M., S. E. O'Connor, M. T. Mazur, C. T. Walsh, and N. L. Kelleher. 2004. Mass spectrometric interrogation of thioester-bound intermediates in the initial stages of epothilone biosynthesis. *Chem. Biol*. 11:327–335.

50. Miller, L. M., M. T. Mazur, S. M. McLoughlin, and N. L. Kelleher. 2005. Parallel interrogation of cIntermediates in the biosynthesis of gramicidin S using high resolution mass spectrometry. *Protein Sci*. 14:2702–2712.

51. Witkowski, A., A. Joshi, and S. Smith. 1996. Fatty acid synthase: in vitro complementation of inactive mutants. *Biochemistry*. 35:10569–10575.

52. Luo, L., and C. T. Walsh. 2001. Kinetic analysis of three activated phenylalanyl intermediates generated by the initiation module PheATE of gramicidin S synthetase. *Biochemistry*. 40:5329–5337.

53. Luo, L., R. M. Kohli, M. Onishi, U. Linne, M. A. Marahiel, and C. T. Walsh. 2002. Timing of epimerization and condensation reactions in nonribosomal peptide assembly lines: kinetic analysis of phenylalanine activating elongation modules of tyrocidine synthetase B. *Biochemistry*. 41:9184–9196.